

Supporting Information

NHC-stabilized Silyl-substituted Silyliumylidene Ions

*Philipp Frisch and Shigeyoshi Inoue**

Table of Contents

1. Experimental Section	2
1.1. General Methods and Instrumentation	2
1.2 Synthesis of Mes–SiCl ₂ H	3
1.3 Synthesis of [^t Bu ₃ Si–Si(IME ₄) ₂]Cl (1)	5
1.4 Synthesis of [^t Bu ₂ MeSi–Si(NHC) ₂]Cl (2a,b)	7
1.5 Synthesis of [Mes–Si(IME ₄) ₂]Cl (3)	13
1.6 NHC exchange reaction of 2b to 2a	16
2. X-ray Crystallographic Data	23
2.1 SC-XRD structure of [^t Bu ₃ Si–Si(IME ₄) ₂]Cl (1)	24
2.2 SC-XRD structure of [^t Bu ₂ MeSi–Si(IME ₄) ₂]Cl (2a)	24
3. References	26

1. Experimental Section

1.1. General Methods and Instrumentation

All reactions were carried out under exclusion of water and oxygen in an atmosphere of argon 4.6 ($\geq 99.996\%$) using standard Schlenk techniques or in a Labstar glovebox from *MBraun* with H_2O and O_2 levels below 0.5 ppm. Glassware was heat dried under vacuum prior to use. Acetonitrile, pyridine, Acetonitrile- d_3 , pyridine- d_5 , fluorobenzene and fluorobenzene- d_5 were refluxed over CaH_2 , distilled under argon, deoxygenated by three freeze-pump-thaw cycles and stored over 3 Å molecular sieve in a glovebox. Diethylether, THF and *n*-hexane were refluxed over sodium/benzophenone, distilled under argon, deoxygenated by three freeze-pump-thaw cycles and stored over 3 Å molecular sieve in a glovebox. C_6D_6 was stirred over Na-K-alloy, distilled under argon, deoxygenated by three freeze-pump-thaw cycles and stored over 3 Å molecular sieve in a glovebox. All NMR samples were prepared under argon in *J. Young* PTFE valve NMR tubes. NMR spectra at ambient temperature (300 K) were recorded on a *Bruker* AV400US or DRX400 (^1H : 400.13 MHz, ^{13}C : 100.62 MHz, ^{29}Si : 79.49 MHz), AVHD300 (^1H : 300.13 MHz) or AV500C (^1H : 500.36 MHz, ^{13}C : 125.83 MHz, ^{29}Si : 99.41 MHz). The ^1H , ^{13}C and ^{29}Si NMR spectroscopic chemical shifts δ are reported in ppm relative to tetramethylsilane. ^1H and ^{13}C NMR spectra are calibrated against the residual proton and natural abundance carbon resonances of the respective deuterated solvent as internal standard (C_6D_6 : $\delta(^1\text{H}) = 7.16$ ppm and $\delta(^{13}\text{C}) = 128.0$ ppm; CD_3CN : $\delta(^1\text{H}) = 1.94$ ppm and $\delta(^{13}\text{C}) = 118.3$ ppm; $\text{C}_6\text{D}_5\text{N}$: $\delta(^1\text{H}) = 8.74$ ppm and $\delta(^{13}\text{C}) = 150.4$ ppm; $\text{C}_6\text{D}_5\text{F}$: $\delta(^1\text{H}) = 6.90$ ppm). ^{29}Si NMR spectra are referenced to the resonance of tetramethylsilane ($\delta = 0$ ppm) as external standard. The following abbreviations are used to describe signal multiplicities: s = singlet, d = doublet, t = triplet, sept = septet, bs = broad signal, m = multiplet. Quantitative elemental analyses (EA) were carried out using a *HEKAtech* EURO EA instrument equipped with a CHNS combustion analyzer at the Laboratory for Microanalysis at the TUM Catalysis Research Center. Melting Points (M.P.) were determined in sealed glass capillaries under inert gas with a *Büchi* M-565 melting point apparatus. ESI-MS spectra were recorded on a *Bruker* HCT Instrument with a dry gas temperature of 300 °C and an injection speed of 240 μLs^{-1} . Unless otherwise stated, all commercially available chemicals were purchased from *abcr* or *Sigma-Aldrich* and used without further purification. The compounds 1,3,4,5-tetramethylimidazol-2-ylidene (IME_4)^{S1}, 1,3-diethyl-4,5-dimethylimidazol-2-ylidene (IEt_2Me_2)^{S1}, Me_3Li ^{S2}, $^t\text{Bu}_3\text{Si-SiCl}_2\text{H}$ ^{S3} and $^t\text{Bu}_2\text{MeSi-SiCl}_2\text{H}$ ^{S4} were prepared as described in the literature.

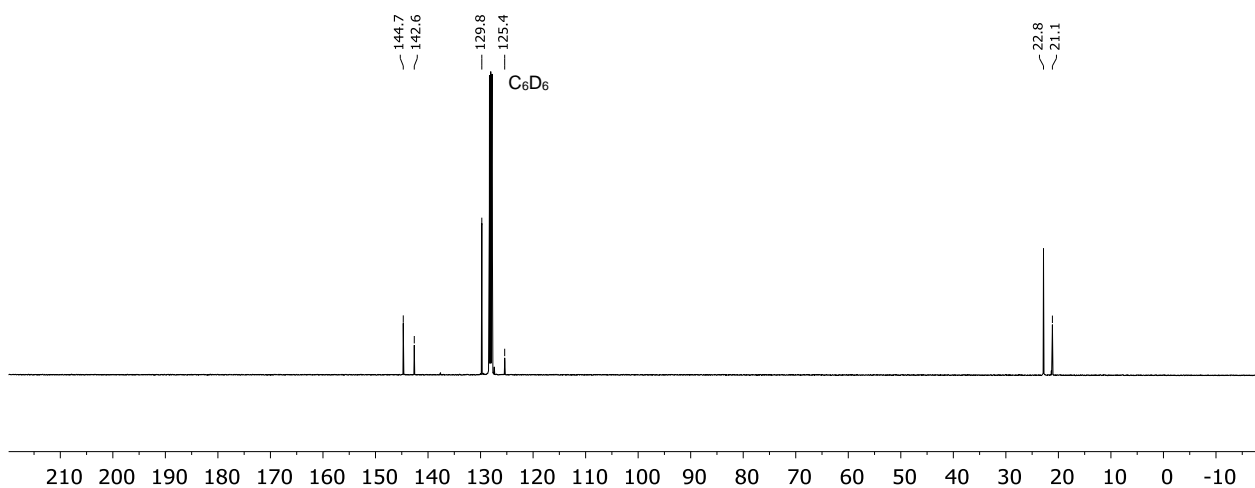


Fig. S2 $^{13}\text{C}\{^1\text{H}\}$ NMR spectrum of Mes-SiCl₂H in C₆D₆ at 300 K.

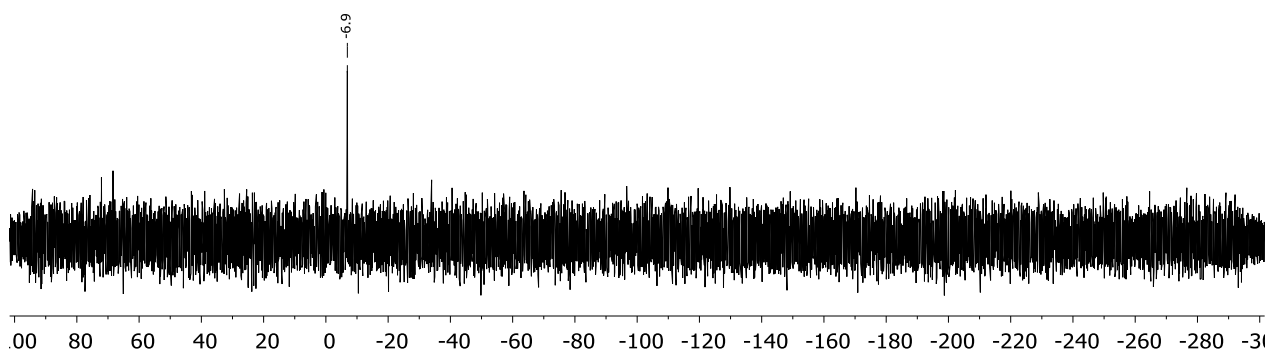
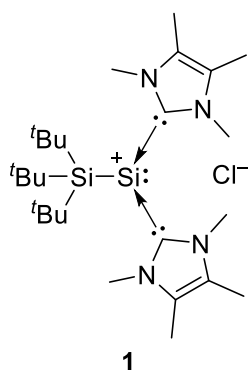


Fig. S3 $^{29}\text{Si}\{^1\text{H}\}$ NMR spectrum of Mes-SiCl₂H in C₆D₆ at 300 K.

1.3 Synthesis of [^tBu₃Si–Si(IMe₄)₂]Cl (**1**)



^tBu₃Si–SiCl₂H (1.00 g, 3.34 mmol, 1.0 eq) was dissolved in 50 mL toluene and cooled to –50 °C. IMe₄ (1.24 g, 10.0 mmol, 3.0 eq) was dissolved in 20 mL toluene and then added dropwise to the silane solution. The mixture was slowly warmed to room temperature overnight. The orange precipitate was collected by filtration, the residue washed with toluene (2×10 mL) and hexane (2×10 mL) and finally extracted with a mixture of toluene and acetonitrile (5:1, 2×30 mL). The solvent was removed under reduced pressure and after drying under vacuum the product **1** (1.11 g, 2.17 mmol, 65%) was isolated as an orange air- and moisture-sensitive powder.

Single crystals suitable for XRD analysis of **1** were obtained by slow diffusion of Et₂O into a concentrated MeCN solution of **1** at –35 °C.

¹H NMR (400 MHz, CD₃CN, 300 K): δ [ppm] = 3.69 (s, 12H, N_{NHC}CH₃), 2.15 (s, 12H, C_{NHC}CH₃), 1.22 (s, 27H, C(CH₃)₃).

¹³C{¹H} NMR (100 MHz, CD₃CN, 300 K): δ [ppm] = 164.1, 128.6, 36.6, 33.0, 26.1, 9.4.

²⁹Si{¹H} NMR (79 MHz, CD₃CN, 300 K): δ [ppm] = 21.8 (SiSi[†]Bu₃), –82.0 (SiSi[‡]Bu₃).

ESI-MS: calculated: 475.36 (C₂₆H₅₁N₄Si₂⁺ = **1** – Cl[–])

measured: 475.2

EA: C₂₆H₅₁ClN₄Si₂ calculated [%]: C (61.07), H (10.05), N (10.96).

measured [%]: C (60.86), H (9.78), N (10.73).

M.P.: 161-162 °C (decomposition, change to red oil).

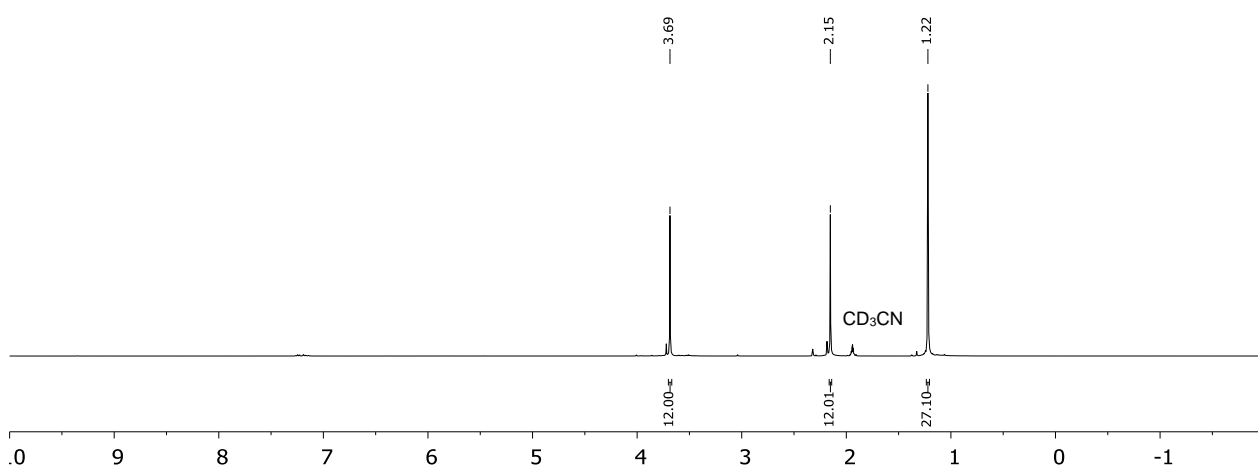


Fig. S4 ¹H NMR spectrum of [^tBu₃Si–Si(IMe₄)₂]Cl (**1**) in CD₃CN at 300 K.

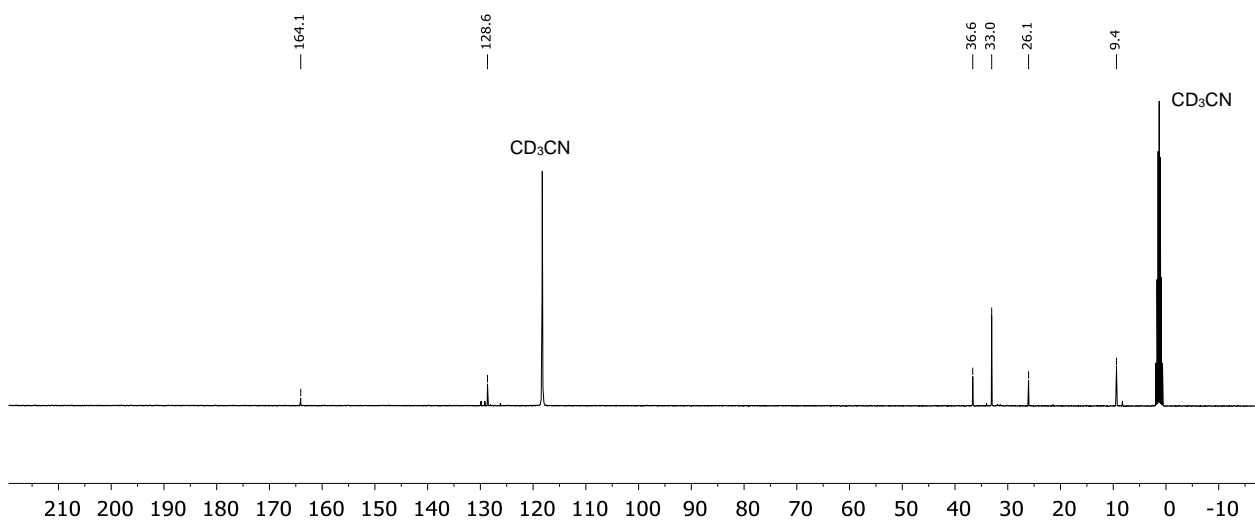


Fig. S5 $^{13}\text{C}\{^1\text{H}\}$ NMR spectrum of $[\text{tBu}_3\text{Si-Si}(\text{IME}_4)_2]\text{Cl}$ (**1**) in CD_3CN at 300 K.

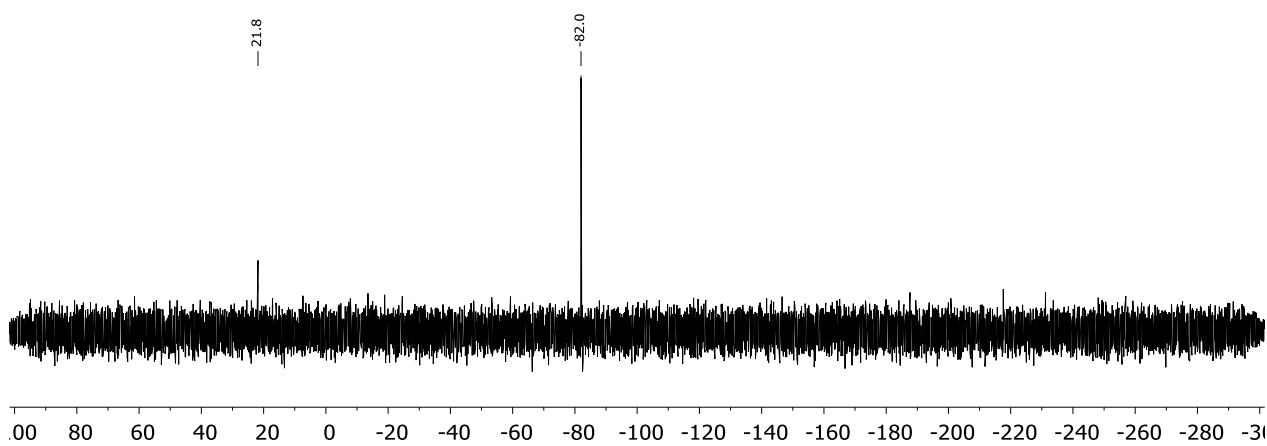


Fig. S6 $^{29}\text{Si}\{^1\text{H}\}$ NMR spectrum of $[\text{tBu}_3\text{Si-Si}(\text{IME}_4)_2]\text{Cl}$ (**1**) in CD_3CN at 300 K.

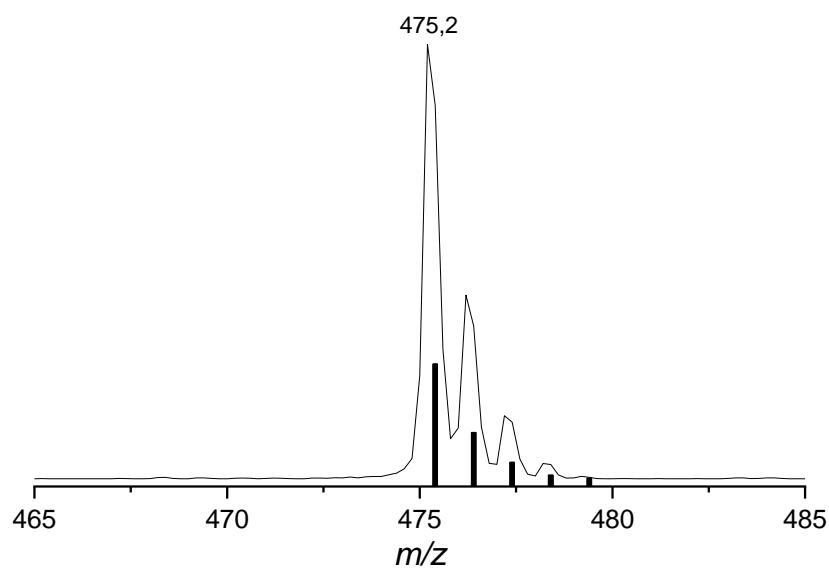
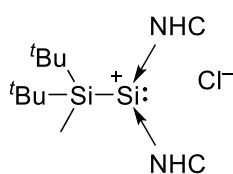


Fig. S7 ESI-MS spectrum (detailed view) of $[\text{tBu}_3\text{Si-Si}(\text{IME}_4)_2]^+$ (**1** - Cl^-) (positive mode, 300 °C, -4000 V; line: measured spectrum; bars: simulated spectrum).

1.4 Synthesis of [^tBu₂MeSi–Si(NHC)₂]Cl (**2a,b**)



2a NHC = IMe₄
2b NHC = IEt₂Me₂

^tBu₂MeSi–SiCl₂H (1.00 g, 3.89 mmol, 1.0 eq) was dissolved in 50 mL toluene and cooled to –50 °C. NHC (11.7 mmol, 3.0 eq) was dissolved in 20 mL toluene and then added dropwise to the silane solution. The mixture was allowed to warm to room temperature overnight. The yellow precipitate was collected by filtration, the residue washed with toluene (2×10 mL) and hexane (2×10 mL), dried under reduced pressure and finally extracted with a mixture of toluene and acetonitrile (8:1, 2×30 mL). The solvent was removed under reduced pressure and after drying under vacuum the products **2a,b** were isolated as yellow to orange air- and moisture-sensitive powders.

[^tBu₂MeSi–Si(IMe₄)₂]Cl (**2a**)

Yield: 1.19 g, 2.54 mmol, 65%.

Single crystals suitable for XRD analysis of **2a** were obtained by storing a concentrated solution of **2a** in 1,2-difluorobenzene at –35 °C.

¹H NMR (400 MHz, CD₃CN, 300 K): δ [ppm] = 3.64 (s, 12H, N_{NHC}CH₃), 2.15 (s, 12H, C_{NHC}CH₃), 0.94 (s, 18H, C(CH₃)₃), 0.40 (SiCH₃).

¹³C{¹H} NMR (100 MHz, CD₃CN, 300 K): δ [ppm] = 163.2, 128.6, 35.8, 29.9, 22.4, 9.3, –1.7.

²⁹Si{¹H} NMR (79 MHz, CD₃CN, 300 K): δ [ppm] = 9.0 (SiSi^tBu₂Me), –90.7 (Si^tBu₂Me).

ESI-MS: calculated: 433.32 (C₂₃H₄₅N₄Si₂⁺ = **2a** – Cl[–])

measured: 433.2

EA: C₂₃H₄₅ClN₄Si₂ calculated [%]: C (58.87), H (9.67), N (11.94).

measured [%]: C (58.62), H (9.63), N (11.77).

M.P.: 158-159 °C (decomposition, change to red oil).

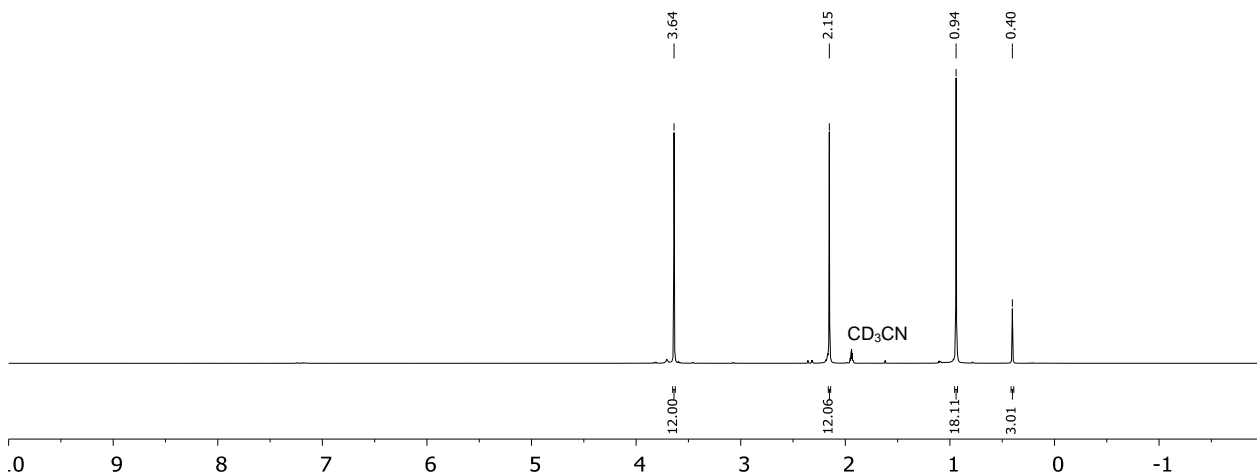


Fig. S8 ¹H NMR spectrum of [^tBu₂MeSi–Si(IMe₄)₂]Cl (**2a**) in CD₃CN at 300 K.

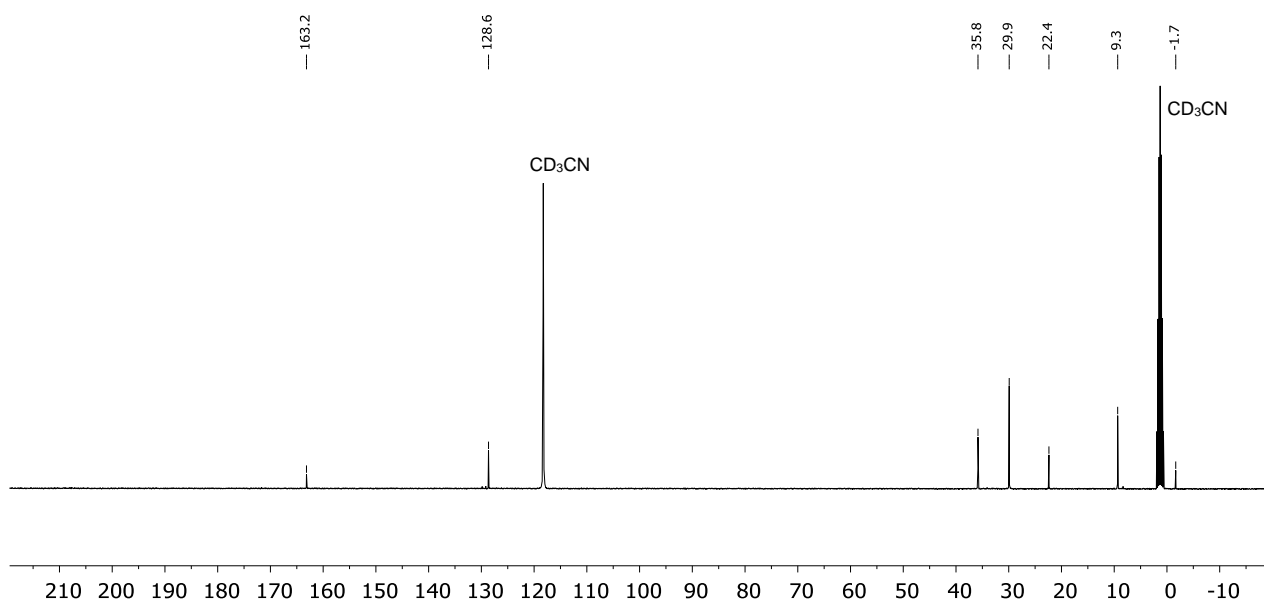


Fig. S9 $^{13}\text{C}\{^1\text{H}\}$ NMR spectrum of $[\text{tBu}_2\text{MeSi-Si}(\text{Ime}_4)_2]\text{Cl}$ (**2a**) in CD_3CN at 300 K.

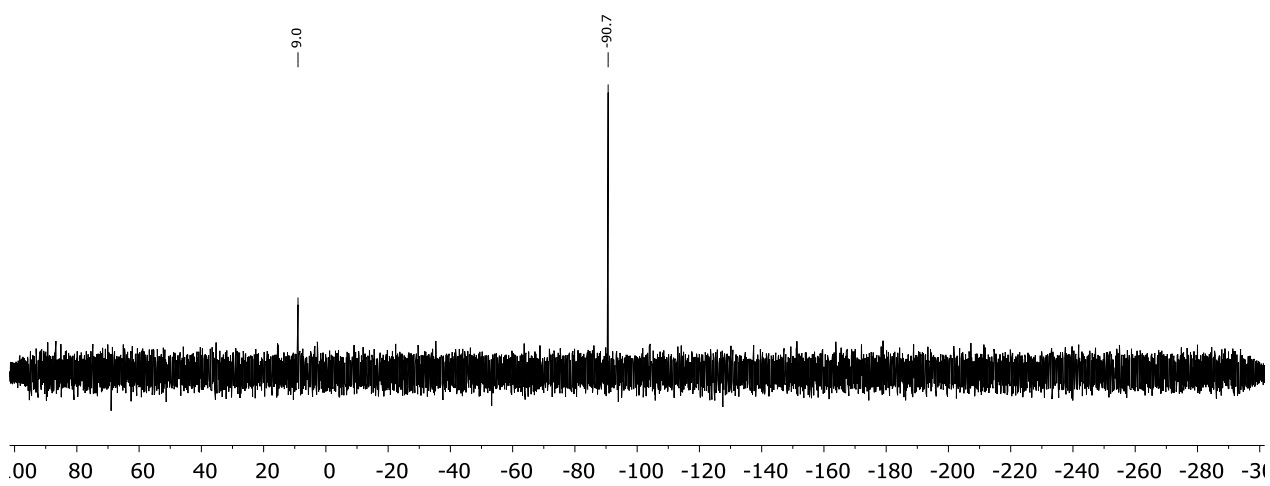


Fig. S10 $^{29}\text{Si}\{^1\text{H}\}$ NMR spectrum of $[\text{tBu}_2\text{MeSi-Si}(\text{Ime}_4)_2]\text{Cl}$ (**2a**) in CD_3CN at 300 K.

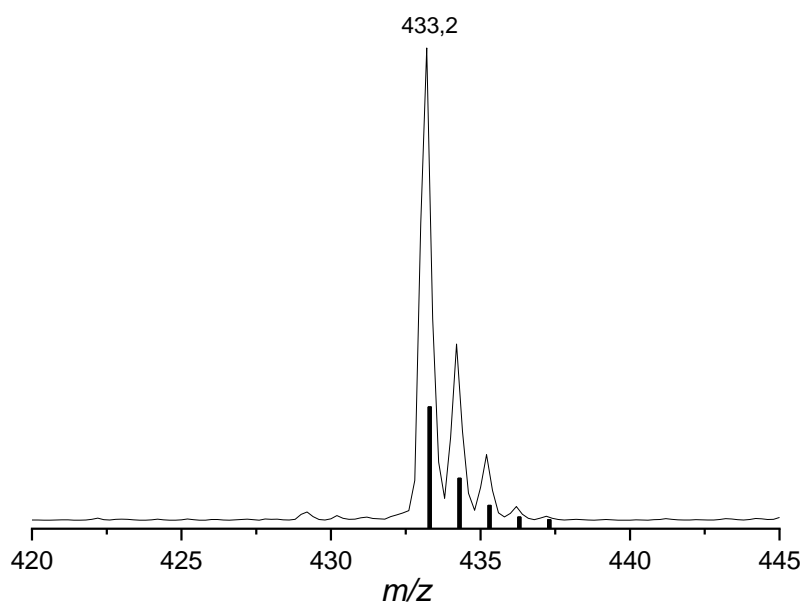


Fig. S11 ESI-MS spectrum (detailed view) of $[\text{tBu}_2\text{MeSi-Si}(\text{Me}_4)_2]^+$ (**2a** - Cl^-) (positive mode, 300 °C, -4000 V; line: measured spectrum; bars: simulated spectrum).

[^tBu₂MeSi–Si(IEt₂Me₂)₂]Cl (2b**)**

Yield: 1.15 g, 2.19 mmol, 56%.

¹H NMR (400 MHz, CD₃CN, 300 K): δ [ppm] = 4.41 (q, *J* = 7.2 Hz, 8H, CH₂CH₃), 2.22 (s, 12H, C_{NHC}CH₃), 1.04 (t, *J* = 7.2 Hz, 12H, CH₂CH₃), 0.92 (s, 18H, C(CH₃)₃), 0.36 (s, 3H, SiCH₃).

¹H NMR (400 MHz, C₆D₅F, 300 K): δ [ppm] = 4.46 (q, *J* = 7.2 Hz, 8H, CH₂CH₃), 2.07 (s, 12H, C_{NHC}CH₃), 1.05-0.99 (m, 30H, CH₂CH₃, C(CH₃)₃), 0.28 (s, 3H, SiCH₃).

Note: The signal for the ethyl wingtip substituent (t, 12H, CH₂CH₃) overlaps with the signal for the ^tBu-substituent (s, 18H, C(CH₃)₃).

¹³C{¹H} NMR (100 MHz, CD₃CN, 300 K): δ [ppm] = 162.3, 129.3, 44.7, 30.0, 22.5, 14.7, 9.4, –2.4.

²⁹Si{¹H} NMR (79 MHz, CD₃CN, 300 K): δ [ppm] = 9.7 (SiSi^tBu₂Me), –86.2 (Si^tSi^tBu₂Me).

ESI-MS: calculated: 489.38 (C₂₇H₅₃N₄Si₂⁺ = **2b** – Cl[–])

measured: 489.2

EA: C₂₇H₅₃CIN₄Si₂ calculated [%]: C (61.73), H (10.17), N (10.66).

measured [%]: C (61.31), H (10.43), N (10.94).

M.P.: 147-148 °C (decomposition, change to red oil).

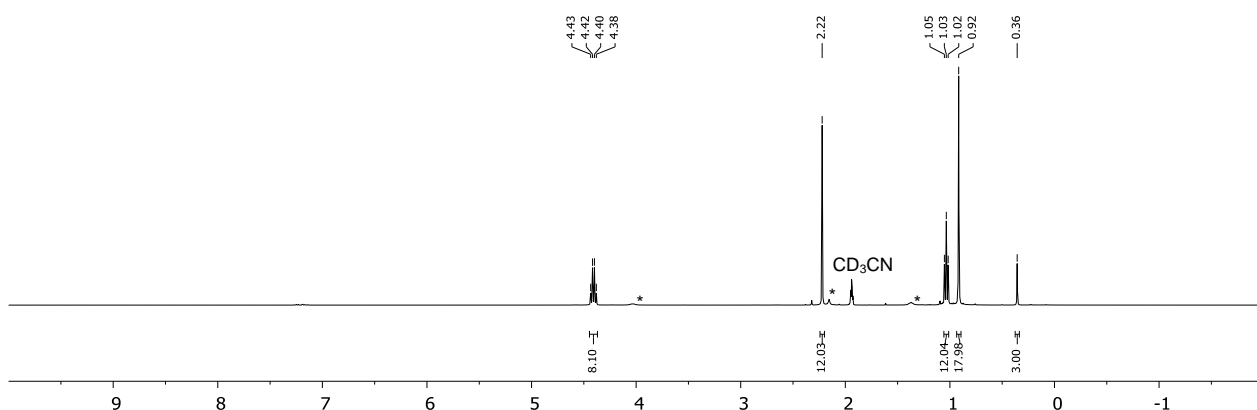


Fig. S12 ¹H NMR spectrum of [^tBu₂MeSi–Si(I_{Et}₂Me₂)₂]Cl (**2b**) in CD₃CN at 300 K. Signals from small amounts of residual I_{Et}₂Me₂·HCl are marked with *.

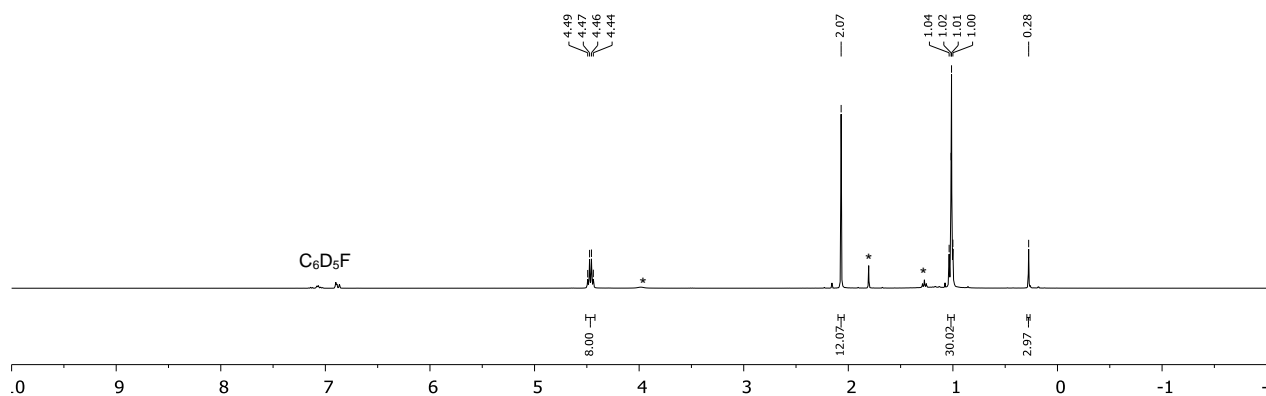


Fig. S13 ^1H NMR spectrum of $[\text{tBu}_2\text{MeSi-Si}(\text{IEt}_2\text{Me}_2)_2]\text{Cl}$ (**2b**) in $\text{C}_6\text{D}_5\text{F}$ at 300 K. Signals from small amounts of residual $\text{IEt}_2\text{Me}_2\cdot\text{HCl}$ are marked with *.

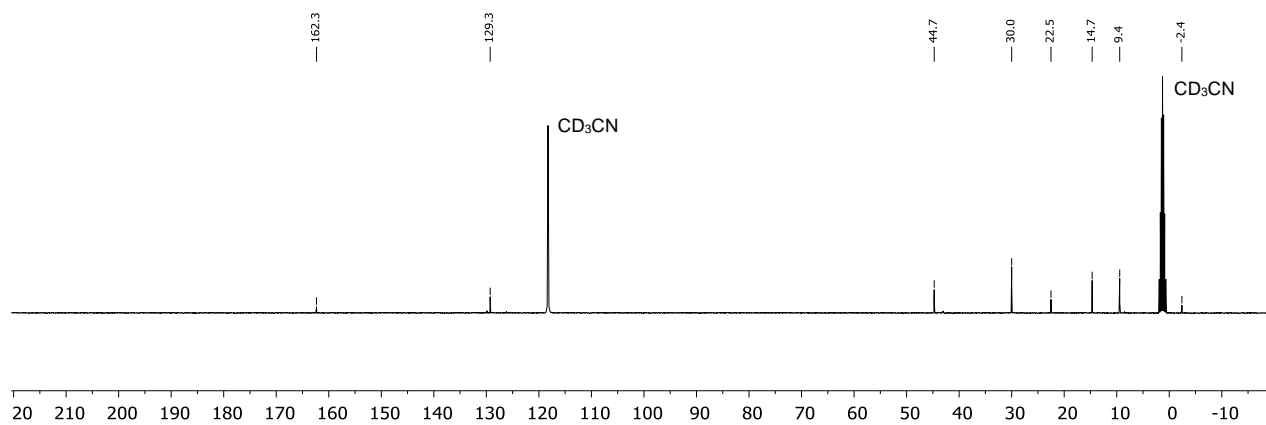


Fig. S14 $^{13}\text{C}\{^1\text{H}\}$ NMR spectrum of $[\text{tBu}_2\text{MeSi-Si}(\text{IEt}_2\text{Me}_2)_2]\text{Cl}$ (**2b**) in CD_3CN at 300 K.

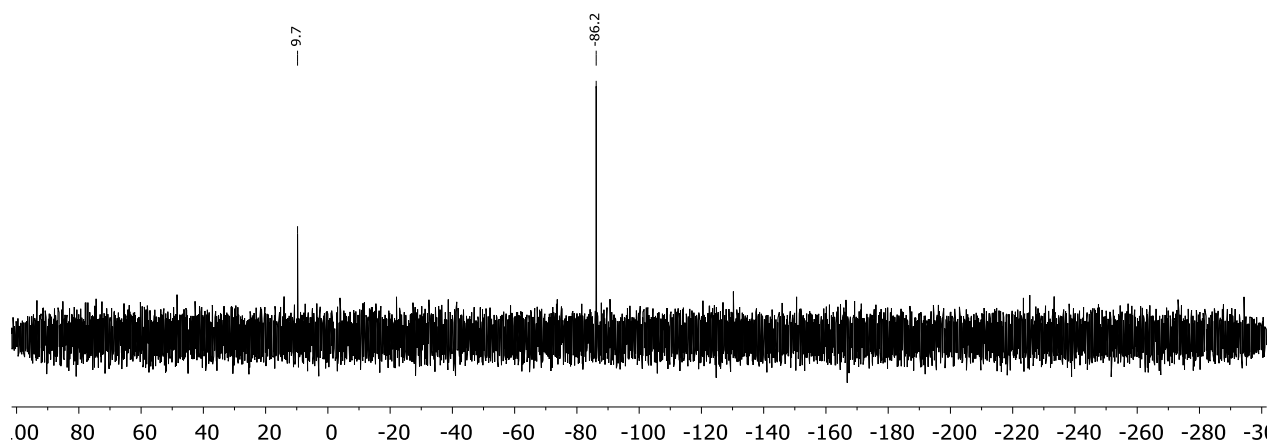


Fig. S15 $^{29}\text{Si}\{^1\text{H}\}$ NMR spectrum of $[\text{tBu}_2\text{MeSi-Si}(\text{IEt}_2\text{Me}_2)_2]\text{Cl}$ (**2b**) in CD_3CN at 300 K.

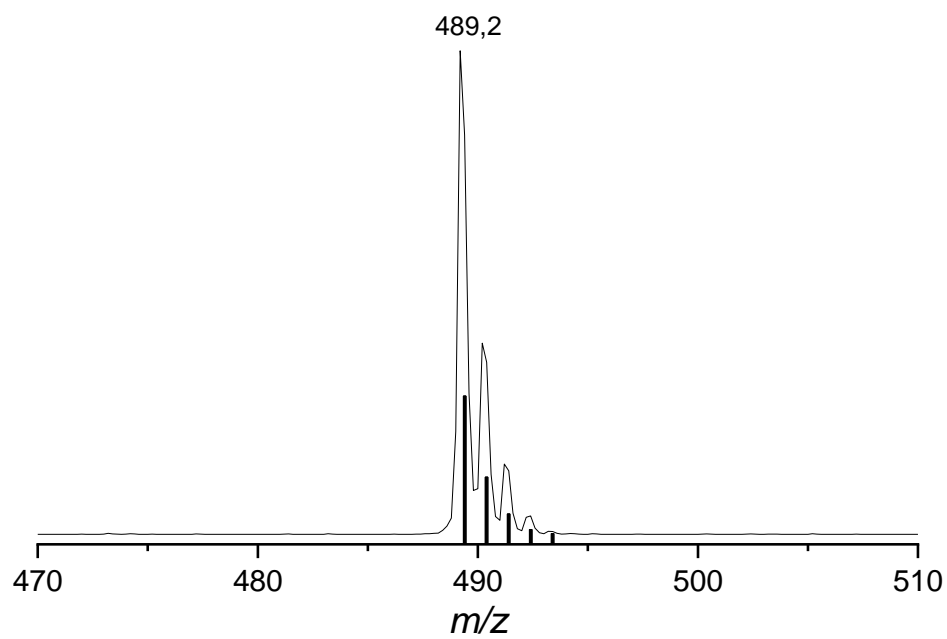
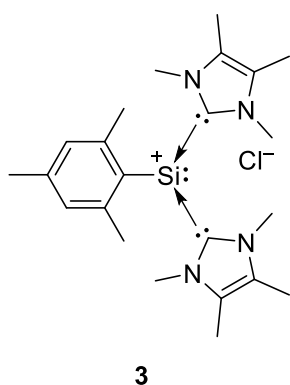


Fig. S16 ESI-MS spectrum (detailed view) of $[\text{Bu}_2\text{MeSi-Si}(\text{IEt}_2\text{Me}_2)_2]^+$ (**2b** - Cl^-) (positive mode, 300 °C, -4000 V; line: measured spectrum; bars: simulated spectrum).

1.5 Synthesis of [Mes–Si(IME₄)₂]Cl (**3**)



Mes–SiCl₂H (1.00 g, 4.56 mmol, 1.0 eq) was dissolved in 60 mL toluene and cooled to –50 °C. IMe₄ (1.70 g, 13.69 mmol, 3.0 eq) was dissolved in 20 mL toluene and then added dropwise to the silane solution. The mixture was allowed to warm to room temperature overnight. The yellow precipitate was collected by filtration, the residue washed with toluene (2×10 mL) and hexane (2×10 mL), dried under reduced pressure and then extracted with pyridine (3×15 mL). The solvent was removed under reduced pressure and after drying under vacuum the product **3** (1.20 g, 2.78 mmol, 61%) was isolated as a pale yellow air- and moisture-sensitive powder.

The compound is very poorly soluble in benzene and well soluble in acetonitrile, pyridine and fluorobenzene. Decomposition occurs in acetonitrile (<4 hours).

¹H NMR (400 MHz, C₅D₅N, 300 K): δ [ppm] = 6.92 (s, 2H, C_{mes}H), 3.68 (s, 12H, N_{NHC}CH₃), 2.29 (s, 6H, C_{mes}CH_{3,ortho}), 2.28 (s, 3H, C_{mes}CH_{3,para}), 2.12 (s, 12H, C_{NHC}CH₃).

¹³C{¹H} NMR (100 MHz, C₅D₅N, 300 K): δ [ppm] = 160.6, 144.8, 137.9, 137.3, 130.0, 128.7, 34.3, 25.2, 21.5, 9.4.

²⁹Si{¹H} NMR (79 MHz, C₅D₅N, 300 K): δ [ppm] = –68.7 (MesSi).

²⁹Si{¹H} NMR (79 MHz, CD₃CN, 300 K): δ [ppm] = –71.2 (MesSi).

ESI-MS: calculated: 311.15 (C₁₄H₂₄N₄SiCl (**3** – Mesityl))

measured: 311.0

Note: The molecular ion peak of **3** – Cl[–] (395.2) could only be observed for a short time upon fast injection. Regular injection speed led to quantitative cleavage of the Si–C bond to the mesityl substituent.

EA: C₂₃H₃₅ClN₄Si calculated [%]: C (64.08), H (8.18), N (13.00).

measured [%]: C (63.62), H (8.02), N (13.32).

M.P.: 180-181 °C (decomposition, color change to black).

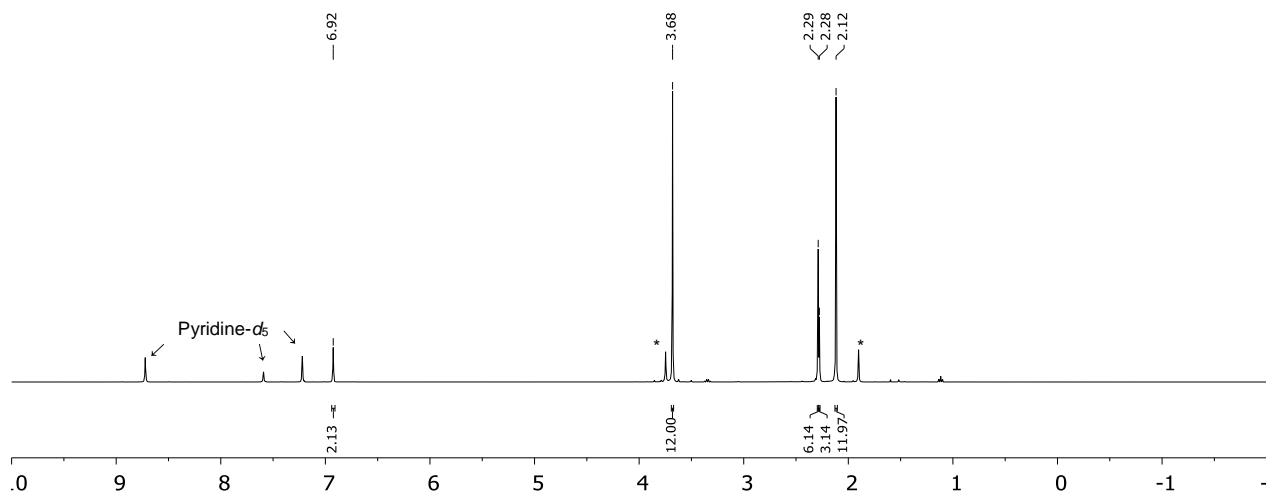


Fig. S17 ^1H NMR spectrum of $[\text{Mes-Si}(\text{IME}_4)_2]\text{Cl}$ (**3**) in pyridine- d_5 at 300 K. Signals from small amounts of residual $\text{IME}_4\text{-HCl}$ are marked with *.

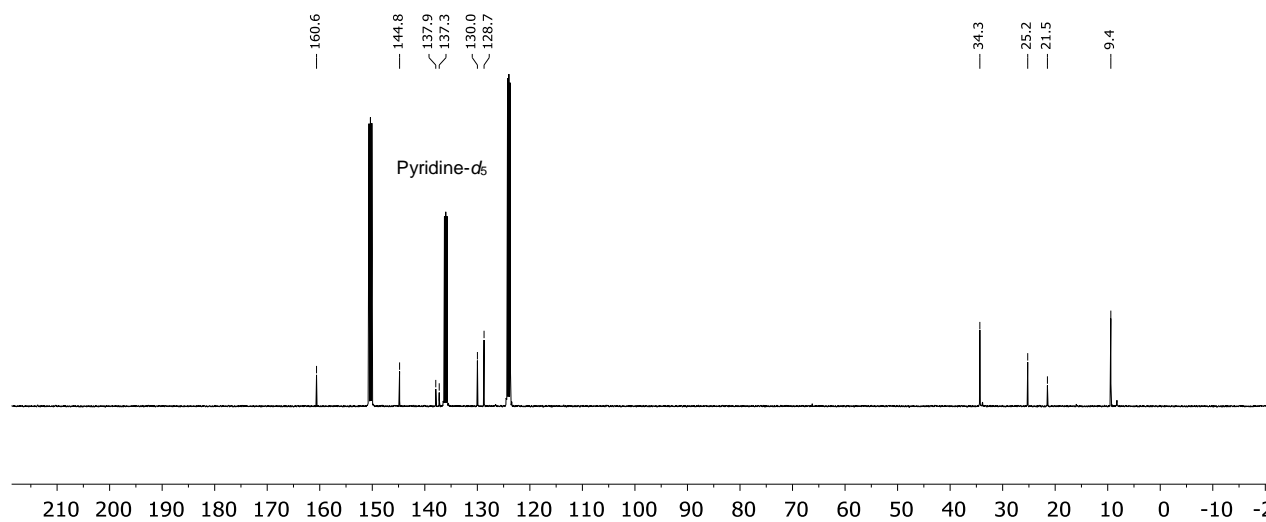


Fig. S18 $^{13}\text{C}\{^1\text{H}\}$ NMR spectrum of $[\text{Mes-Si}(\text{IME}_4)_2]\text{Cl}$ (**3**) in pyridine- d_5 at 300 K.

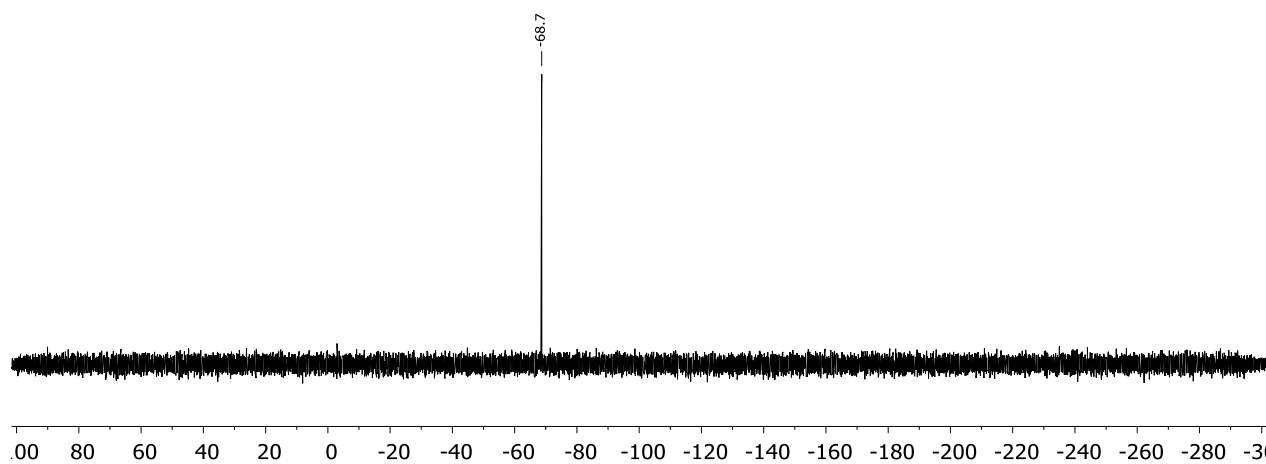


Fig. S19 $^{29}\text{Si}\{^1\text{H}\}$ NMR spectrum of $[\text{Mes-Si}(\text{IME}_4)_2]\text{Cl}$ (**3**) in pyridine- d_5 at 300 K.

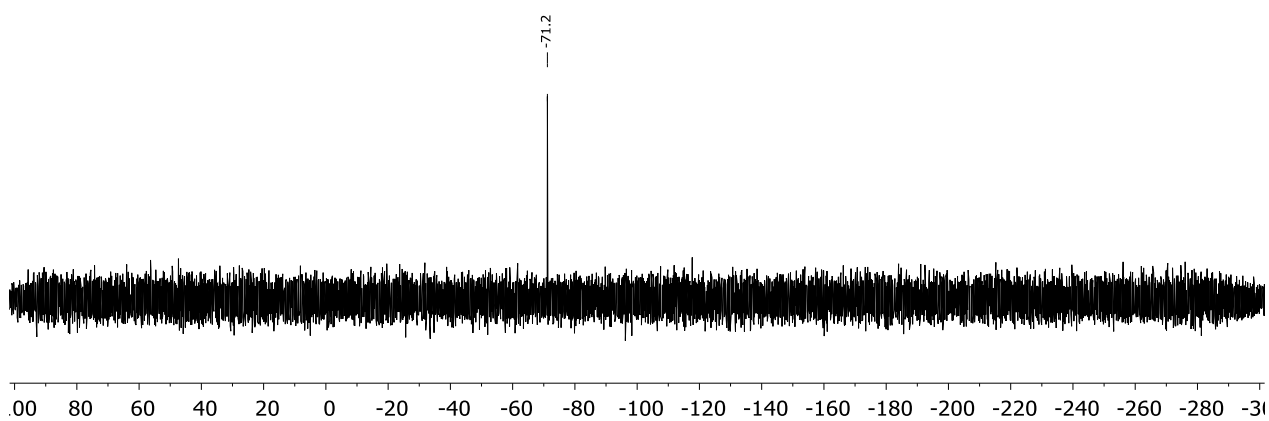


Fig. S20 $^{29}\text{Si}\{^1\text{H}\}$ NMR spectrum of $[\text{Mes-Si}(\text{IME}_4)_2]\text{Cl}$ (**3**) in CD_3CN at 300 K.

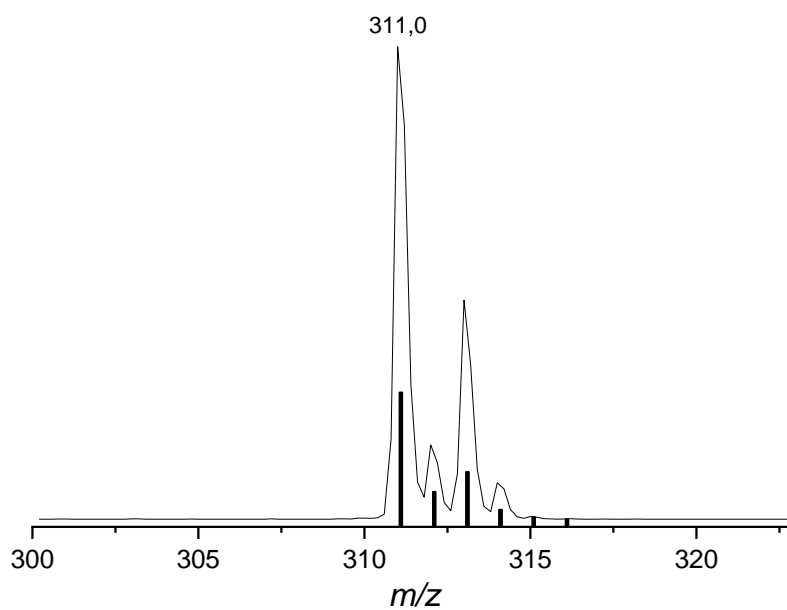
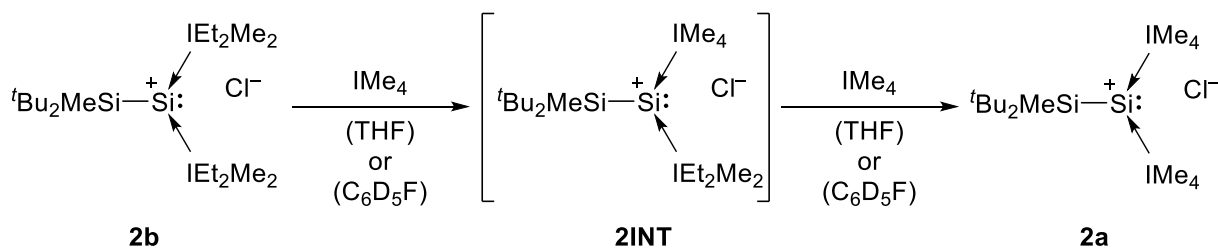


Fig. S21 ESI-MS spectrum (detailed view) of $[\text{Si}(\text{IME}_4)_2]\text{Cl}$ (**3** – Mes) (positive mode, 300 °C, –4000 V; line: measured spectrum; bars: simulated spectrum).

1.6 NHC exchange reaction of **2b** to **2a**



Procedure for the NHC exchange reaction:

$[\text{tBu}_2\text{MeSi}-\text{Si}(\text{IEt}_2\text{Me}_2)_2]\text{Cl}$ (**2b**) (50.0 mg, 95.2 μmol , 1.0 eq) was dissolved in 2 mL THF and a solution of IME_4 (23.6 mg, 190.3 μmol , 2.0 eq) in 0.5 mL THF was added dropwise. Rapid formation of a yellow precipitate was observed, which was collected by filtration and washed with THF (2 \times 2 mL) and hexane (1 \times 1 mL) and after drying under vacuum product **2a** (36.6 mg, 78.0 μmol , 82%) was isolated as a yellow powder. Analytical data in CD_3CN are the same as previously mentioned (*cf.* section 1.4)

Procedure for the NHC exchange reaction (NMR scale):

$[\text{tBu}_2\text{MeSi}-\text{Si}(\text{IEt}_2\text{Me}_2)_2]\text{Cl}$ (**2b**) (20.0 mg, 38.1 μmol , 1.0 eq) and $\text{Si}(\text{TMS})_4$ (12.2 mg, 38.1 μmol , 1.0 eq) were dissolved in 0.3 mL $\text{C}_6\text{D}_5\text{F}$, transferred to a J. Young NMR tube and then frozen at -78°C . IME_4 (9.5 mg, 76.1 μmol , 2.0 eq) was dissolved in 0.2 mL $\text{C}_6\text{D}_5\text{F}$ and then slowly added to the frozen solution. The frozen mixture was then allowed to warm up slightly, then shaken strongly and several ^1H NMR measurements were taken immediately followed by ^1H NMR measurements in selected intervals (*cf.* Table S1). $\text{Si}(\text{TMS})_4$ was used as internal standard.

Fig. S22 and Fig. S23 show the time resolved NMR data in $\text{C}_6\text{D}_5\text{F}$ with 2.5 eq of IME_4 . The third set of signals belongs to the intermediate **2INT** $[(\text{tBu}_2\text{MeSi}-\text{Si}(\text{IME}_4)(\text{IEt}_2\text{Me}_2)]\text{Cl}$. While we have been unable to isolate **2INT** in a clean fashion, in addition to the observations made in the ^1H NMR measurements, we were able to investigate the reaction mixture with ^{29}Si NMR (Fig. S24). As expected, the ^{29}Si NMR resonances of **2INT** (9.2 ppm ($^t\text{Bu}_2\text{MeSiSi}$), -89.2 ppm ($^t\text{Bu}_2\text{MeSiSi}$)) fall between that of **2b** (9.8 ppm ($^t\text{Bu}_2\text{MeSiSi}$), -86.2 ppm ($^t\text{Bu}_2\text{MeSiSi}$)) and **2a** (9.0 ppm ($^t\text{Bu}_2\text{MeSiSi}$), -90.7 ppm ($^t\text{Bu}_2\text{MeSiSi}$)).

To record a ^{29}Si NMR of the mixture in CD_3CN for better comparability, $\text{C}_6\text{H}_5\text{F}$ was removed quickly from the reaction mixture after roughly 20 minutes of reaction time. The residue was dissolved in CD_3CN , the suspension was filtered and a ^{29}Si NMR was measured immediately.

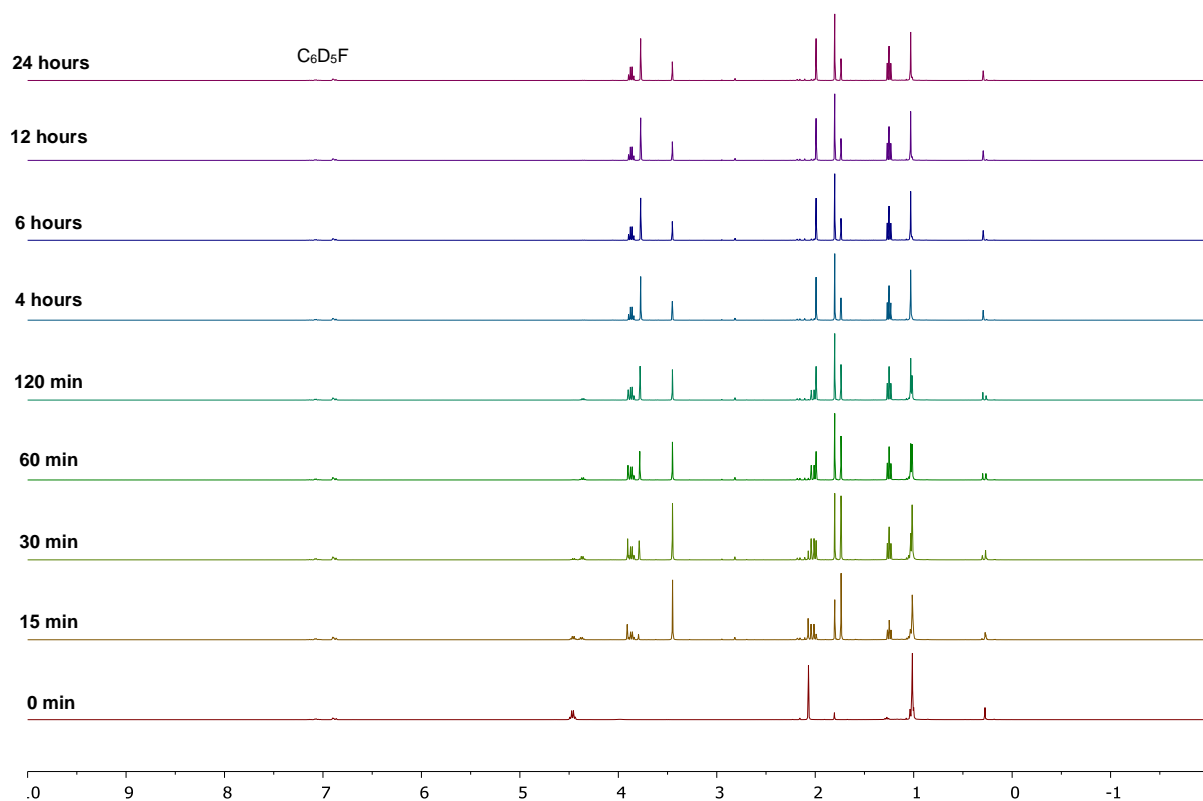


Fig. S22 Time resolved ^1H NMR spectra (overview) of the NHC exchange of **2b** with excess IMe_4 to **2a**.

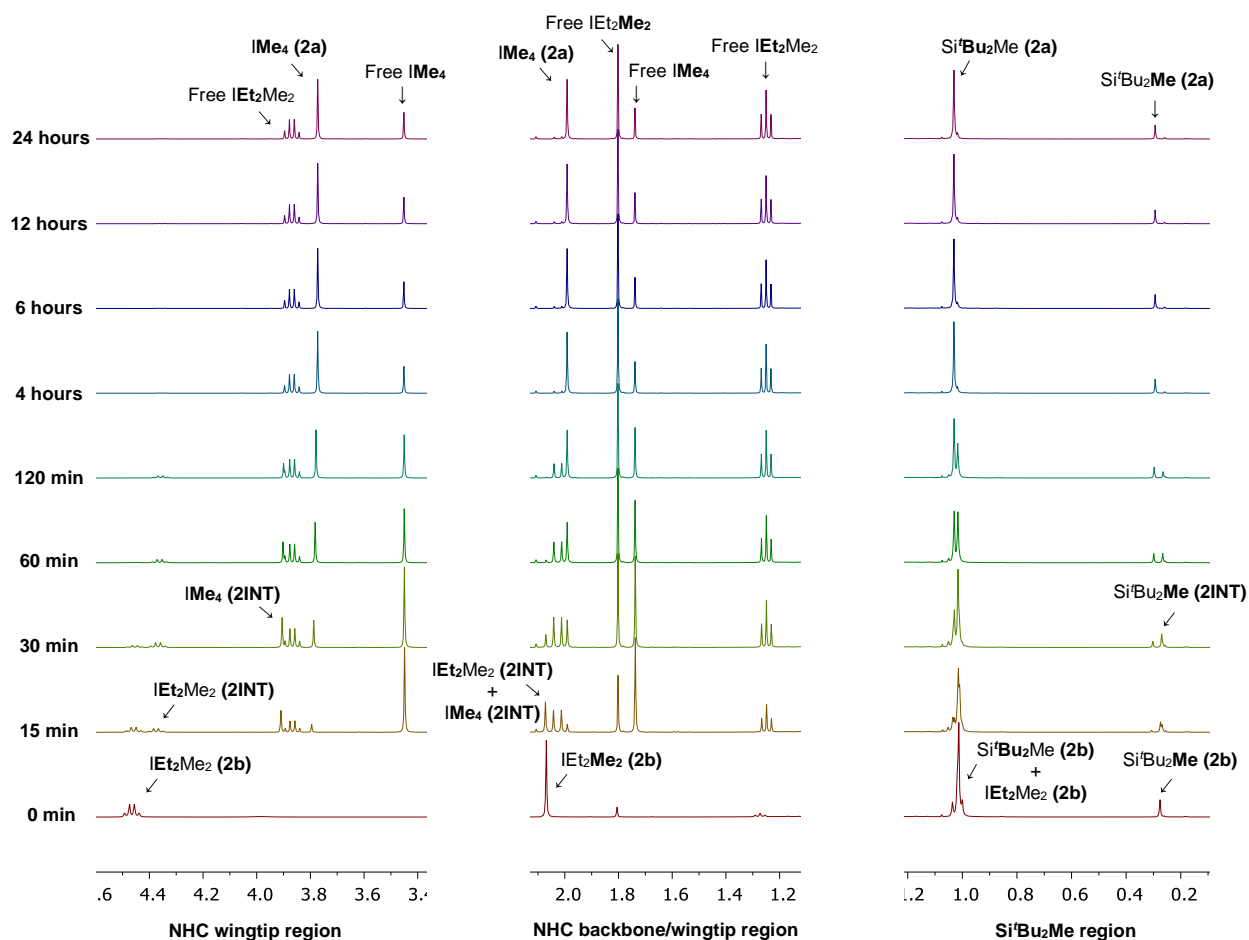


Fig. S23 Time resolved ^1H NMR spectra (detail view) of the NHC exchange of **2b** with excess IMe_4 to **2a**.

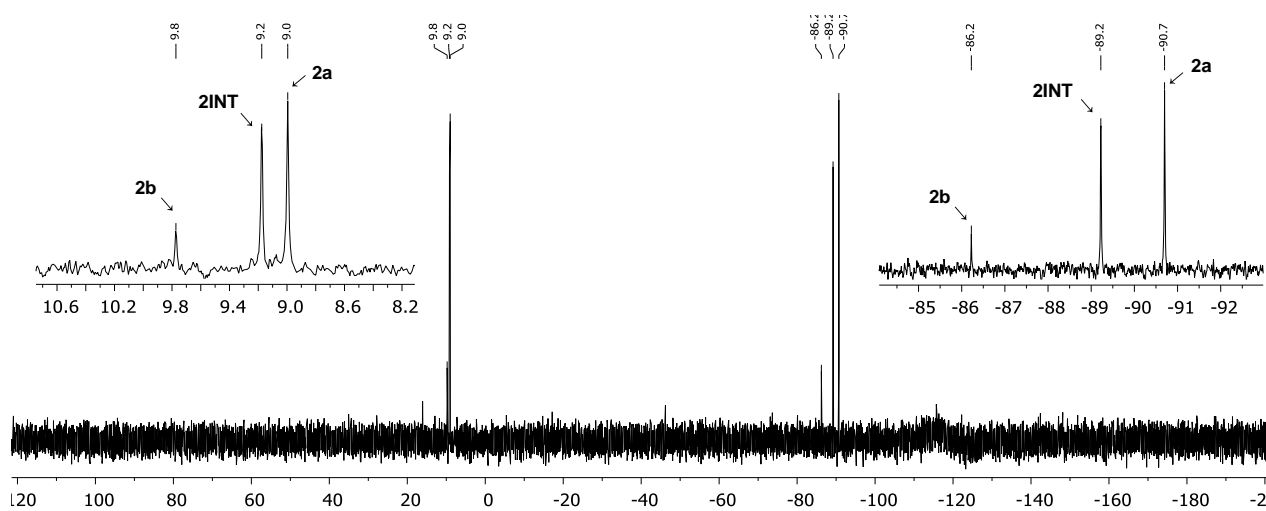


Fig. S24 $^{29}\text{Si}\{^1\text{H}\}$ NMR spectrum in CD_3CN of the reaction mixture of the NHC exchange of **2b** to **2a** via the intermediate **2INT**.

Table S1 Relative [%] and absolute [mmol/L] molar concentrations of **2b**, **2INT** and **2a** by time as determined by ¹H NMR.

t [min]	Δt [min]	2b		2INT		2a	
		[%]	[mmol/L]	[%]	[mmol/L]	[%]	[mmol/L]
0	–	100.0	76.1	0.0	0.0	0.0	0.0
3	3	71.9	54.7	26.9	20.5	1.2	0.9
5	2	58.1	44.2	39.2	29.8	2.8	2.1
7	2	48.7	37.0	46.5	35.4	4.9	3.7
9	2	40.6	30.9	52.2	39.8	7.2	5.5
11	2	34.0	25.9	56.0	42.7	10.0	7.6
13	2	29.5	22.4	58.5	44.5	12.1	9.2
16	3	24.0	18.2	60.8	46.3	15.2	11.6
18	2	20.2	15.4	61.7	47.0	18.1	13.8
20	2	17.6	13.4	62.1	47.3	20.3	15.5
22	2	14.7	11.1	62.0	47.2	23.4	17.8
27	5	10.0	7.6	60.3	45.9	29.7	22.6
37	10	5.9	4.5	55.6	42.3	38.5	29.3
47	10	3.5	2.7	49.4	37.6	47.1	35.8
58	11	2.5	1.9	42.9	32.7	54.6	41.5
72	14	1.5	1.2	35.0	26.7	63.4	48.3
87	15	1.2	0.9	28.8	22.0	70.0	53.3
102	15	0.9	0.7	24.5	18.7	74.6	56.8
117	15	0.8	0.6	21.2	16.1	78.0	59.4
132	15	0.6	0.5	18.4	14.0	81.0	61.7
147	15	0.3	0.3	16.0	12.2	83.6	63.6
177	30	0.0	0.0	13.3	10.1	86.7	66.0
208	31	–	–	11.2	8.5	88.8	67.6
238	30	–	–	10.3	7.8	89.7	68.3
268	30	–	–	9.7	7.4	90.3	68.7
298	30	–	–	9.2	7.0	90.8	69.1
328	30	–	–	8.9	6.8	91.1	69.4
358	30	–	–	8.5	6.4	91.5	69.7
388	30	–	–	8.0	6.1	91.9	70.0
448	60	–	–	7.7	5.9	92.3	70.3
508	60	–	–	7.6	5.8	92.4	70.4
568	60	–	–	7.5	5.7	92.5	70.5
628	60	–	–	7.3	5.6	92.7	70.6

Plotting the relative molar concentrations vs. the reaction time (Fig. S25 (overview), Fig. S26 (**2b**), Fig. S27 (**2INT**), Fig. S29 (**2a**)) allows easy observation of the reaction progress.

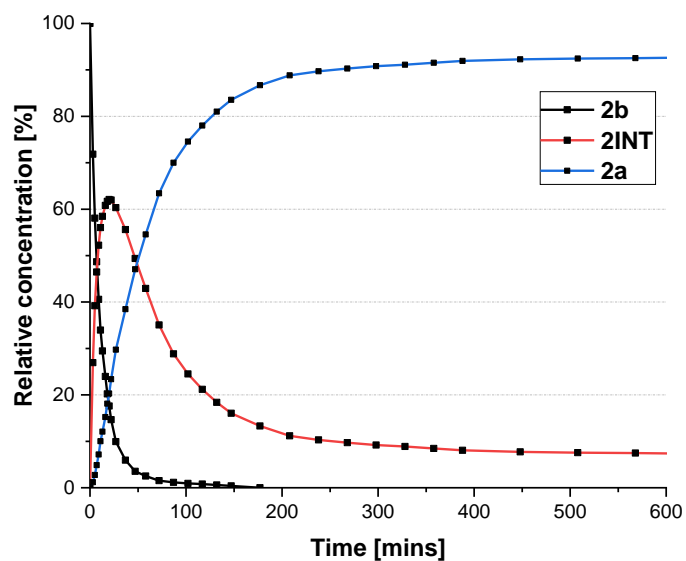


Fig. S25 Plot of the relative concentration of **2b**, **2INT** and **2a** vs. the time in the NHC exchange reaction of **2b** to **2a** via **2INT**.

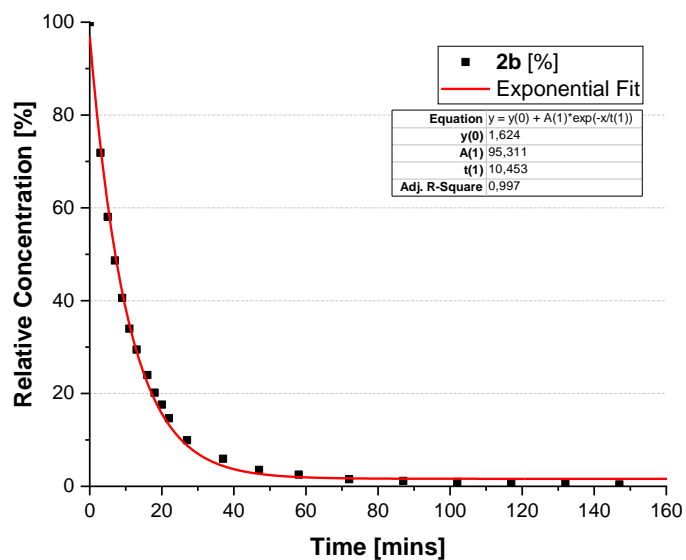


Fig. S26 Plot of the relative concentration of **2b** vs. time in the NHC exchange reaction of **2b** to **2a** via **2INT**.

The kinetics of a reaction can be deduced from a linear correlation between either $1/c_{2b}$ vs. the time (2nd order kinetics) or $\ln(c_{2b})$ vs. the time (1st order kinetics). However, the first NHC exchange from **2b** to **2INT** is heavily influenced by the concentration of IMe_4 , which changes during the reaction because of the additional consumption of IMe_4 from the second step of the reaction. Choosing a smaller time window to determine the reaction order does not allow reliable conclusions to be drawn from the data. We therefore looked at the second step of the reaction from **2INT** to **2a** in a time period where the overwhelming majority of **2b** had already been consumed (Fig. S27 and Fig. S28).

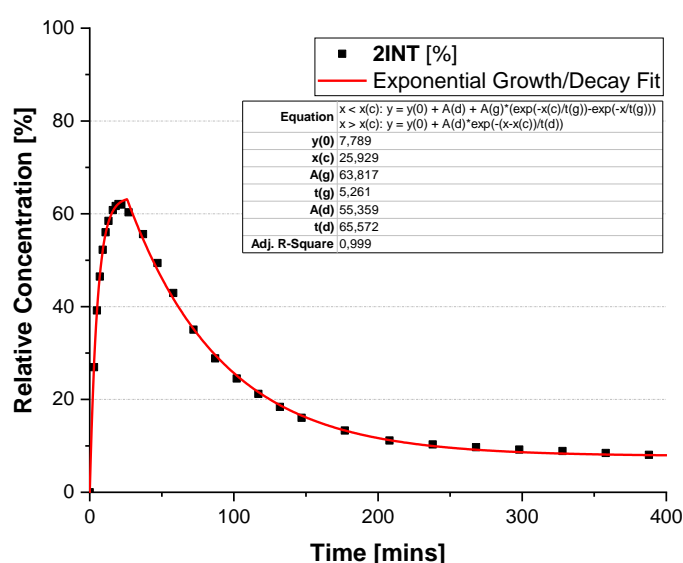


Fig. S27 Plot of the relative concentration of **2INT** vs. time in the NHC exchange reaction of **2b** to **2a** via **2INT**.

Plotting $1/c_{2INT}$ vs. the reaction time shows a linear correlation (Fig. S28, excluding the startup period where **2INT** is formed from **2b**), which indicates the reaction follows 2nd order kinetics. The rate constant of the second exchange reaction is $0.558 \text{ L} \cdot \text{mol}^{-1} \cdot \text{min}^{-1}$. The first exchange reaction should exhibit the same reaction kinetics.

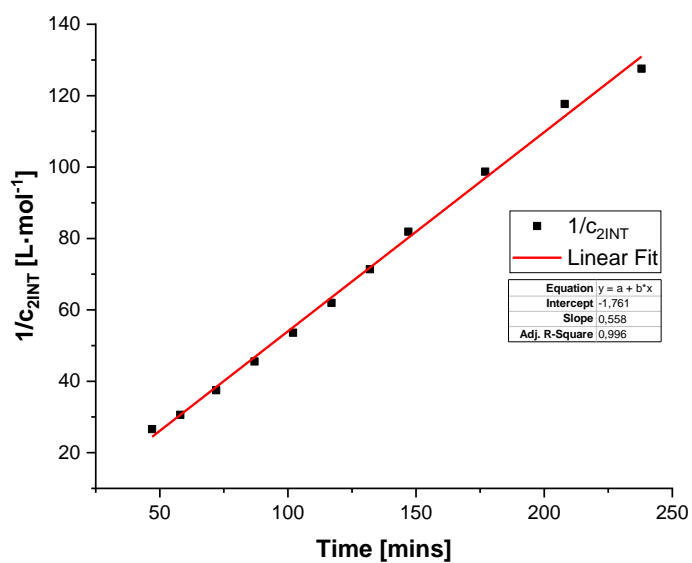


Fig. S28 Plot of $1/c_{2INT}$ vs. time in the NHC exchange reaction of **2b** to **2a** via **2INT**.

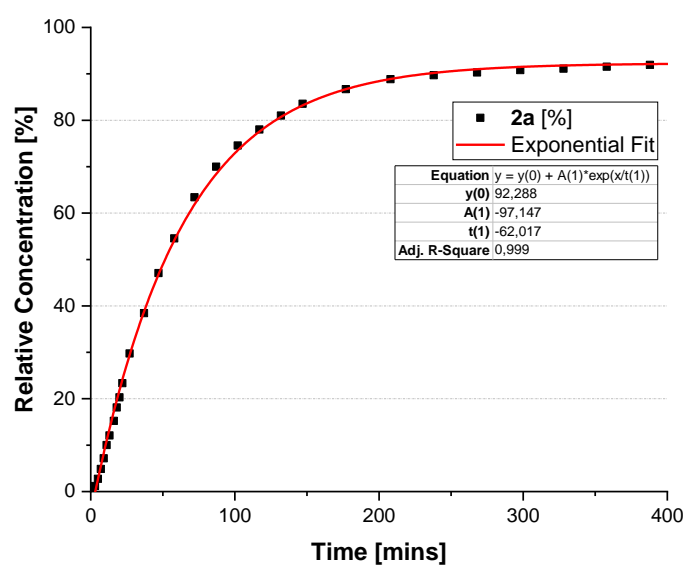


Fig. S29 Plot of the relative concentration of **2a** vs. the time in the NHC exchange reaction of **2b** to **2a** via **2INT**.

2. X-ray Crystallographic Data

General Information

The X-ray intensity data of **1** and **2a** were collected on an X-ray single crystal diffractometer equipped with a CMOS detector (Bruker Photon-100), a rotating anode (Bruker TXS) with MoK α radiation ($\lambda = 0.71073 \text{ \AA}$) and a Helios mirror optic by using the APEX III software package.^{S5} The measurements were performed on single crystals coated with the perfluorinated ether Fomblin® Y. The crystals were fixed on the top of a micro sampler, transferred to the diffractometer and frozen under a stream of cold nitrogen. A matrix scan was used to determine the initial lattice parameters. Reflections were merged and corrected for Lorenz and polarization effects, scan speed, and background using SAINT.^{S6} Absorption corrections, including odd and even ordered spherical harmonics were performed using SADABS.^{S6} Space group assignments were based upon systematic absences, E statistics, and successful refinement of the structures. Structures were solved by direct methods with the aid of successive difference Fourier maps, and were refined against all data using the APEX III software in conjunction with SHELXL-2014^{S7} and SHELXLE.^{S8} All H atoms were placed in calculated positions and refined using a riding model, with methylene and aromatic C–H distances of 0.99 and 0.95 \AA , respectively, and $U_{\text{iso}}(\text{H}) = 1.2 \cdot U_{\text{eq}}(\text{C})$. Full-matrix least-squares refinements were carried out by minimizing $\Delta w(F_o^2 - F_c^2)^2$ with SHELXL-97 weighting scheme.^{S9} Neutral atom scattering factors for all atoms and anomalous dispersion corrections for the non-hydrogen atoms were taken from International Tables for Crystallography.^{S10} The images of the crystal structures were generated by Mercury.^{S11} The CCDC numbers CCDC-1914471 (**1**) and CCDC-1914472 (**2a**) contain the supplementary crystallographic data for the structures. These data can be obtained free of charge from the Cambridge Crystallographic Data Centre *via* <https://www.ccdc.cam.ac.uk/structures/>.

2.1 SC-XRD structure of [^tBu₃Si–Si(IME₄)₂]Cl (1)

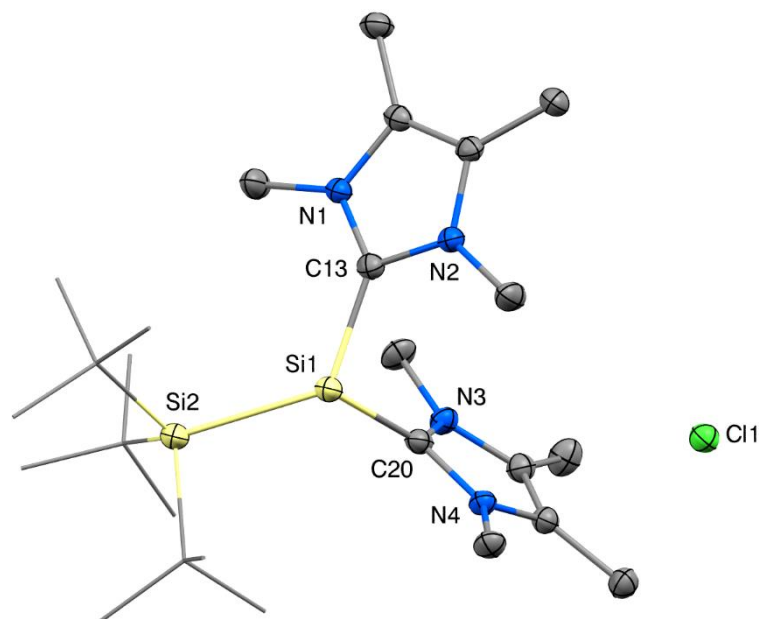


Fig. S30 Ellipsoid plot (50% probability level) of the molecular structure of compound **1**. Hydrogen atoms and solvent molecules are omitted for clarity. Selected bond lengths [Å] and angles [°]: Si1–Si2 2.424(1), Si1–C13 1.937(2), Si1–C20 1.943(3), Si2–Si1–C13 122.1(1), Si2–Si1–C20 113.5(1), C13–Si1–C20 93.1(1).

2.2 SC-XRD structure of [^tBu₂MeSi–Si(IME₄)₂]Cl (2a)

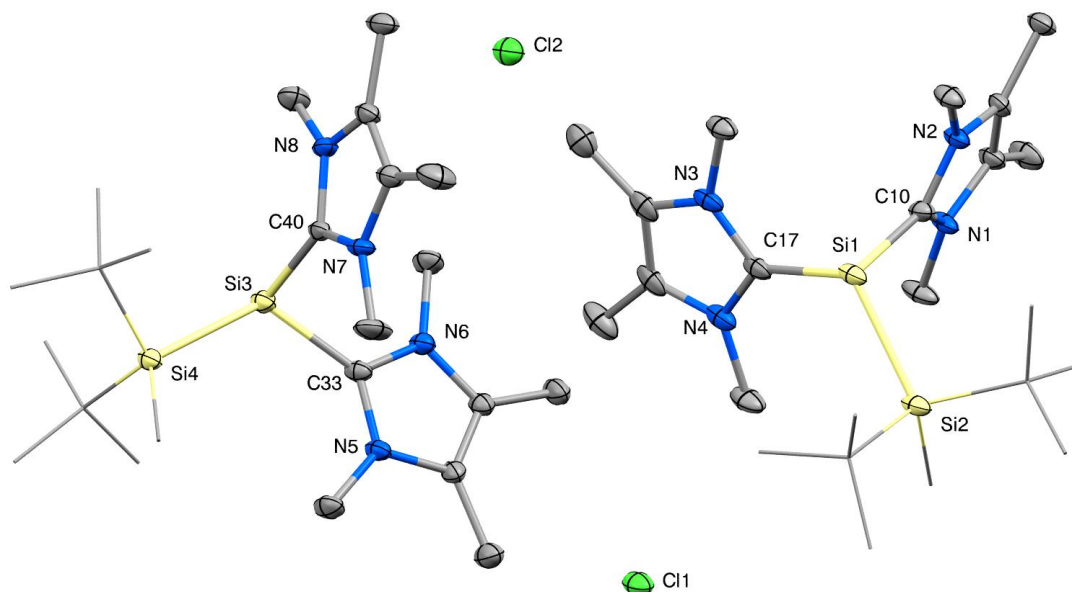


Fig. S31 Ellipsoid plot (50% probability level) of the molecular structure of compound **2a**. Hydrogen atoms and solvent molecules are omitted for clarity. Selected bond lengths [Å] and angles [°]: Si1–Si2 2.388(1), Si1–C10 1.943(2), Si1–C17 1.945(3), Si2–Si1–C10 107.4(1), Si2–Si1–C17 117.9(1), C10–Si1–C17 93.6(1), Si3–Si4 2.396(1), Si3–C33 1.940(3), Si3–C40 1.947(3), Si4–Si3–C33 117.5(1), Si4–Si3–C40 105.8(1), C33–Si3–C40 94.1(1).

Table S2 Crystal data and structural refinement parameters for compounds **1** and **2a**.

Compound #	1	2a
Chemical formula	C ₃₀ H ₅₇ Cl ₁ N ₆ Si ₂	C ₅₂ H ₉₄ Cl ₂ F ₂ N ₈ Si ₄
Formula weight	593.45	1052.62
Temperature	100(2) K	100(2) K
Wavelength	0.71073 Å	0.71073 Å
Crystal size	0.178 x 0.243 x 0.472 mm	0.199 x 0.226 x 0.272 mm
Crystal habit	clear orange fragment	clear yellow fragment
Crystal system	trigonal	triclinic
Space group	R -3	P -1
Unit cell dimensions	a = 45.605(5) Å, α = 90° b = 45.605(5) Å, β = 90° c = 9.2968(11) Å, γ = 120°	a = 11.0482(19) Å, α = 66.805(5)° b = 17.171(3) Å, β = 74.978(5)° c = 21.066(4) Å, γ = 88.261(6)°
Volume	16745(4) Å ³	3536.2(11) Å ³
Z	6	4
Density (calculated)	1.059 g/cm ³	0.989 g/cm ³
Absorption coefficient	0.193 mm ⁻¹	0.199 mm ⁻¹
F(000)	5832	1140
Diffractometer	Bruker D8 Venture	Bruker D8 Venture
Radiation source	TXS rotating anode, Mo	TXS rotating anode, Mo
Theta range for data collection	2.25 to 25.35°	2.22 to 25.68°
Index ranges	-54 ≤ h ≤ 54 -54 ≤ k ≤ 54 -11 ≤ l ≤ 11	-13 ≤ h ≤ 13 -20 ≤ k ≤ 20 -25 ≤ l ≤ 25
Reflections collected	226492	63614
Independent reflections	6800 [R(int) = 0.0716]	13410 [R(int) = 0.0838]
Coverage of independent reflections	99.9%	99.9%
Absorption correction	Multi-Scan	Multi-Scan
Max. and min. transmission	0.9660 and 0.9140	0.9610 and 0.9470
Refinement method	Full-matrix least-squares on F ²	Full-matrix least-squares on F ²
Refinement program	SHELXL-2016/6 (Sheldrick, 2016)	SHELXL-2016/6 (Sheldrick, 2016)
Function minimized	Σ w(F _o ² - F _c ²) ²	Σ w(F _o ² - F _c ²) ²
Data / restraints / parameters	6800 / 0 / 371	13410 / 132 / 716
Goodness-of-fit on F²	1.104	1.024
Δ/σ_{max}	0.002	0.001
Final R indices	5960 data; I > 2σ(I) R1 = 0.0432, wR2 = 0.1240 all data R1 = 0.0512, wR2 = 0.1296	9895 data; I > 2σ(I) R1 = 0.0521, wR2 = 0.1114 all data R1 = 0.0802, wR2 = 0.1207
Weighting scheme	w = 1/[σ ² (F _o ²) + (0.0634P) ² + 45.3570P] where P = (F _o ² + 2F _c ²)/3	w = 1/[σ ² (F _o ²) + (0.0378P) ² + 3.4602P] where P = (F _o ² + 2F _c ²)/3
Largest diff. peak and hole	0.857 and -0.262 eÅ ⁻³	0.728 and -0.336 eÅ ⁻³
R.M.S. deviation from mean	0.061 eÅ ⁻³	0.056 eÅ ⁻³

3. References

- S1 N. Kuhn and T. Kratz, *Synthesis*, 1993, **1993**, 561-562.
- S2 A. Hübner, T. Bernert, I. Sängler, E. Alig, M. Bolte, L. Fink, M. Wagner and H.-W. Lerner, *Dalton Trans.*, 2010, **39**, 7528-7533.
- S3 N. Wiberg, W. Niedermayer, H. Nöth, J. Knizek, W. Ponikwar and K. Polborn, *Z. Naturforsch. B.*, 2000, **55**, 389.
- S4 V. Y. Lee, K. Takanashi, R. Kato, T. Matsuno, M. Ichinohe and A. Sekiguchi, *J. Organomet. Chem.*, 2007, **692**, 2800-2810.
- S5 *APEX suite of crystallographic software*, APEX 3 version 2015.5-2; Bruker AXS Inc.: Madison, Wisconsin, USA, 2015.
- S6 *SAINT*, Version 7.56a and *SADABS* Version 2008/1; Bruker AXS Inc.: Madison, Wisconsin, USA, 2008.
- S7 G. M. Sheldrick, *SHELXL-2014*, University of Göttingen, Göttingen, Germany, 2014.
- S8 C. B. Hübschle, G. M. Sheldrick and B. Dittrich, *J. Appl. Cryst.*, 2011, **44**, 1281-1284.
- S9 G. M. Sheldrick, *SHELXL-97*, University of Göttingen, Göttingen, Germany, 1998.
- S10 A. J. C. Wilson, *International Tables for Crystallography*, Vol. C, Tables 6.1.1.4 (pp. 500-502), 4.2.6.8 (pp. 219-222), and 4.2.4.2 (pp. 193-199); Kluwer Academic Publishers: Dordrecht, The Netherlands, 1992.
- S11 C. F. Macrae, I. J. Bruno, J. A. Chisholm, P. R. Edgington, P. McCabe, E. Pidcock, L. Rodriguez-Monge, R. Taylor, J. van de Streek and P. A. Wood, *J. Appl. Cryst.*, 2008, **41**, 466-470.